JOURNAL OF MATERIALS SCIENCE 32 (1997) 1613–1622

Mechanisms of particulate filled polypropylene finite plastic deformation and fracture

I. L. DUBNIKOVA, V. G. OSHMYAN, A. YA. GORENBERG
Institute of Chemical Physics, Russian Academy of Sciences, 4 Kosygin St., 117977, Moscow, Russia

The plastic deformation and fracture of aluminium hydroxide filled polypropylene has been investigated. A transition between two mechanisms with an increase of the filler volume fraction has been observed. Below a critical filler volume content $\phi_{cr} \approx 20$ vol% (designated region 1) adhesive failure processes and polymer deformation in the neighbourhoods of different particles occur in an uncorrelated manner. Above this critical value (designated region 2) exfoliation along the surface of the initial portion of inclusions causes the formation of craze-like deformation zones transverse to the direction of the loading. The concentration of craze-like zones is essentially determined by the filler content and the level of interphase interaction which in turn depends on the particle size. In region 1 deformation occurs in a macro heterogeneous way with the formation and growth of a neck. The elongation to break decreases with an increase in the mean diameter of the filler phase. At $\phi > \phi_{cr}$ composites, filled with small particles, fail in quasi brittle manner with the formation of a short and narrow neck. In contrast to the case for a small filler concentration, an increase of the inclusion size leads to an increase in the ultimate elongation and a tendency to macro homogeneous yielding. An explanation of the observed behaviour is proposed based on a change in adhesive failure conditions with filler content and size.

1. Introduction

Polyolefines can undergo large (up to 700%) plastic deformations. The addition of rigid inclusions leads to the hardening of composites, but unfortunately it is accompanied by a drop in the ultimate elongation. One of the main requirements of particulate filled polymers (PFP) is an increase or conservation of their stiffness without any essential loss in plastic ability.

The change in the elastic moduli of a composite with filler volume content (ϕ) can be reasonably well theoretically predicted in the cases of perfect and also weak adhesive interactions. Certain regularities in a composite plastic characteristics were found in the case of small strains [1, 2]. However, to date no detailed mechanisms to explain PFP finite deformation are available.

Numerous experimental investigations have highlighted the dependencies of a PFPs finite deformation and fracture parameters on: (i) the polymer matrix properties [3–5], (ii) the uniformity of the particle dispersion [4] and their content and size [4–6], and (iii) the level of adhesive interaction [7]. A sharp plastic–brittle transition with filling to a certain filler fraction ϕ_{br} has been reported for particulate filled HDPE [5]. ϕ_{br} rises with an increase in the polymer matrix tendency to strain hardening. Ultimate strains (ε_b) may be optimized by judicious choice of the size of the inclusions for a given polymer matrix [4–6]. The more uniform the particle distribution, the higher are the ε_b values obtained [4]. The increase of adhesive strength by means of chemical modification of the filler surface leads to a significant drop in ε_b [7].

Macroscopic yielding of PFP on the basis of HDPE and PP, is anticipated by the formation of pores as a result of debonding processes, as is shown in the scanning electron microscopy observations reported in reference [8]. As will be discussed at a later point in this paper, these processes essentially determine the plastic behaviour of the composite. Adhesive failure regularities have been investigated by the authors both experimentally and theoretically and are reported in references [9, 10], for low glass bead contents. One of the main conclusions of this study is a drop in the debonding stress (σ_d) (value of the specific load sufficient for the interphase exfoliation) with an increase in the diameter of the particles.

The goal of the present paper is the clarification of the PFP large plastic deformation and fracture mechanisms and an explanation of the observed transitions with the change of filler content and size. The experiments were performed on polypropylene (PP)–$Al(OH)_3$ composite samples. Narrow filler fractions of different mean diameters were used. The uniformity of the particle dispersion and the stability of the polymer molecular and supermolecular structure were controlled. The modification of the interface by liquid silicone was used in order to weaken any adhesive interaction.

0022–2461

The correlations between the debonding micro processes and characteristics of the composites macroscopic yielding are clarified.

2. Experimental procedure

Isotactic PP whose atactic fraction did not exceed 2% was used as the matrix. The polymer molecular weight characteristics, measured by the GPC method, were: $\bar{M}_w = 630\,000$, $\bar{M}_n = 180\,000$ and $\bar{M}_w/\bar{M}_n = 3.5$. Aluminium hydroxide $Al(OH)_3$ powder with a density of 2.4 g cm^{-3} was used as the filler. Four fractions of mean ($\bar{d}$), minimum (d_{min}) and maximum (d_{max}) diameters were used: 1 (0.5–1.5), 2.5 (1.5–5), 8 (4–16) and 25 (5–50) μm.

The composites were prepared in a Brabender mixing chamber at 190 °C and the duration of the mixing was 10 min. Calcium stearate (2 wt % of the filler content) was added in order to avoid filler aggregation. The destruction of the polymer was prevented by the addition of topanol (0.3 wt %) and dilauriltiodipropionate (0.5 wt %). For comparison purposes nonfilled PP underwent the same treatment in the mixer in order to test the conservation of its mechanical parameters. The filler contents used were in the range 0–70 wt % (0–47 vol %).

The specimens for mechanical testing were prepared by moulding at 190 °C under a pressure of 10 MPa which was maintained during the sample cooling. The room temperature drawing of the blade-shaped samples was performed using an Instron-1122 at a strain rate of 0.67, l per min.

The structure of the composites in both the unstressed and deformed state was observed by scanning electron microscopy (SEM) using a JSM-35C microscope. The supermolecular structure of the polymer in the composites was investigated by SEM and wide-angle X-ray diffraction techniques.

3. Results and discussion

3.1. Filler space distribution and polymer matrix morphology

The control of the structure of the PP–$Al(OH)_3$ composites was achieved by the quantitative analysis of micrographs of the low temperature fracture surfaces. It was observed that in the range of filler fraction studied, the specimens are characterized by a relatively uniform particle distribution in the matrix. In addition, the mean values of the particle diameters in the composites are the same as $\bar{d}$ in the initial fractions and also agglomerates with a size larger than d_{max} were not observed.

The mechanical properties of semi-crystalline polymers are essentially determined by their supermolecular structure. Thus it was necessary to check the influence of the inclusions on the polymer matrix morphology. SEM observations showed that the PP spherolite diameter is almost independent of the particle content and size. The stability of the polymer crystallinity (about 64%) and crystallite size was established by wide-angle X-ray diffraction.

3.2. Two mechanisms of PFP finite plastic deformation

In order to clarify the PFP plastic flow behaviour it is obviously important to study any effect due to the particle volume content and size on the ultimate strain at uniaxial stretching. The ε_b–ϕ dependencies measured for a number of particle sizes are represented in Fig. 1. Two specific filler content regions are clearly observed. Region 1 ($\phi < 20$ vol %) is characterized by a larger drop in ε_b with an increase in ϕ for the case of larger particles. On the other hand, in region 2 ($\phi > 20$ vol %) an increase in the filler mean diameter leads to a rise in the ultimate strain. In the case of small particle ($\bar{d} = 1$ and 2.5 μm) the composites quickly lose their large plastic deformation behaviour at ϕ values $\simeq 20$ vol % and break in a quasi-brittle manner. The concentration dependence of ε_b becomes smoother for $\bar{d} = 8$ μm and grows in the interval $15 < \phi < 35$ vol % for $\bar{d} = 25$ μm. It should be noted that this behaviour is rather surprising and has not been previously reported. Thus, the measurement of ultimate elongation has revealed the existence of a critical filler content $\phi_{cr} \simeq 20$ vol % at which inversion of the ε_b–$\bar{d}$ dependency occurs.

Microscopy observations of the deformed samples and measurements of the cross-sectional areas confirm the existence of the critical transition. Below ϕ_{cr} (region 1) the samples deform macro heterogeneously by necking (Fig. 2a, Table I). Localization of the yielding is accompanied by the whitening of the neck region. Analysis of the microstructure of the deformed samples was performed by SEM. Representative surface micrographs of the differently deformed regions in the specimen containing 4 vol % of $Al(OH)_3$ ($\bar{d} = 8$ μm) are shown in Fig. 3(a and b). It is seen that in spite of the macro heterogeneous behaviour, plastic deformation occurs in a micro homogeneous manner: the highly stretched neck is characterized by fundamentally drawn polymer and uniformly distributed well developed pores containing inclusions. The relative lengthening of all pores in the direction of the

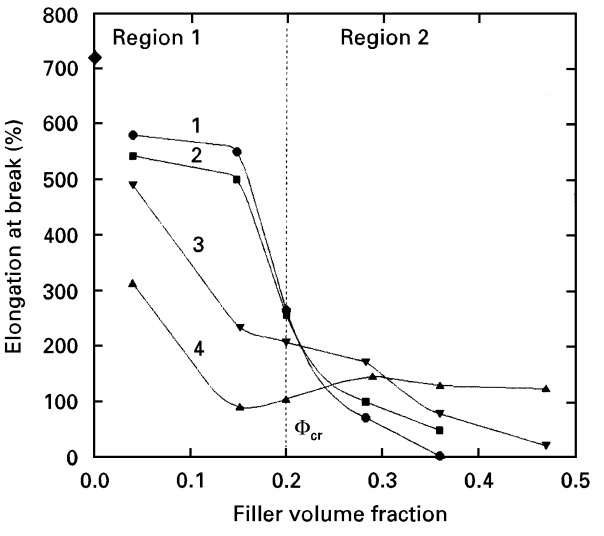

Figure 1 Elongations at break as a function of filler volume fraction for different particle size: (1) $\bar{d} = 1$, (2) 2.5, (3) 8 and (4) 25 μm. (◆) – unfilled PP.

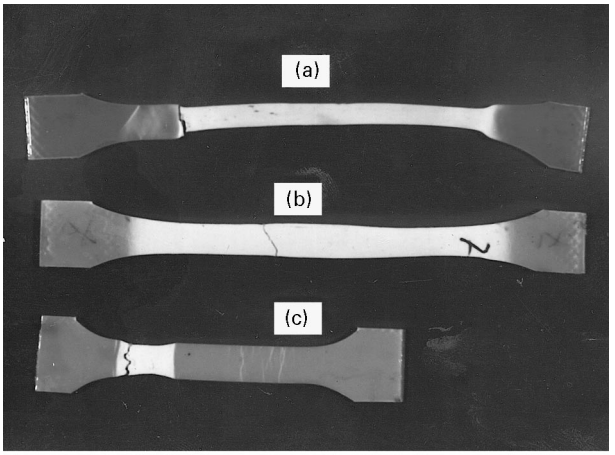

Figure 2 Photographs of the deformed samples, containing (a) 4 vol % of particles with $\bar{d} = 8$ μm, (b) 36 vol % of particles with $\bar{d} = 25$ μm and (c) $\bar{d} = 2.5$ μm.

loading is very close to the mean draw ratio in the neck. Thus on the basis of this analysis of deformed specimens at filler contents less than ϕ_{cr} we suggest the mechanism to be a micro homogeneous one. This means that adhesive failure processes and matrix deformation in the vicinities of different inclusions occur independently without the formation of any kind of specific zones.

Above ϕ_{cr} (region 2) the deformation of the composite occurs without any essential shrinkage of the cross-sectional area (Fig. 2(b and c) Table I). Plastic flow is accompanied by a noticeable whitening of the material similar to that observed in region 1, however, a completely different microstructure is formed. Micrographs of the samples with $\phi = 28$ vol % are shown in

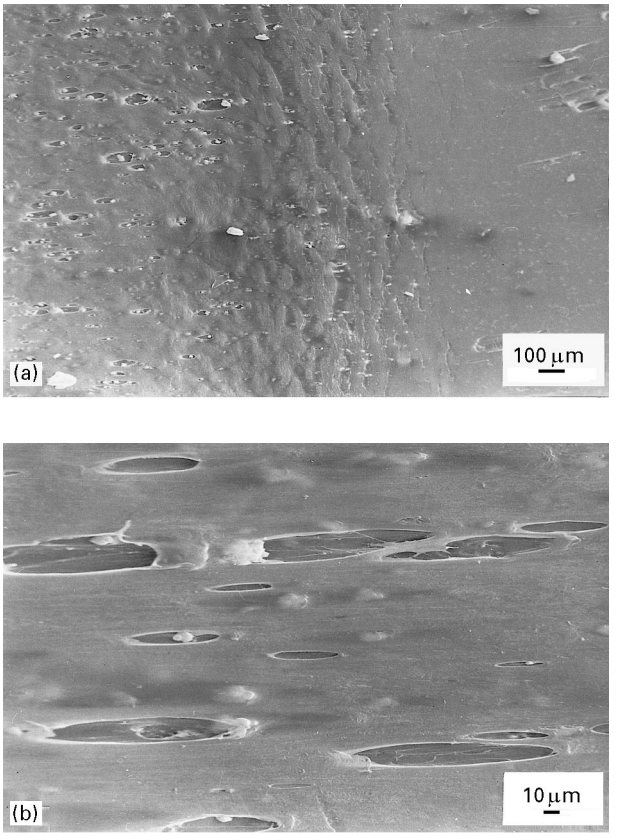

Figure 3 SEM micrographs of the surfaces of the deformed compositions, containing 4 vol % of a filler with $\bar{d} = 8$ μm: (a) in the region of the neck shoulders and (b) the region of the neck.

Fig. 4(a and b) ($\bar{d} = 1$ μm), Fig. 5(a and b) ($\bar{d} = 8$ μm) and Fig. 6(a and b) ($\bar{d} = 25$ μm). A common feature in these micrographs is the alternation of weakly and highly deformed areas. High resolution micrographs

TABLE I Effect of filler content and particle size on the mechanical properties of PP–$Al(OH)_3$ composites

$\bar{d}$ (μm)	ϕ (vol %)	E (MPa)	σ_e (MPa)	σ_y (MPa)	ε_y (%)	ε_{pl} (%)	σ_{pl} (MPa)	σ_n^{tr} (MPa)	σ_{br} (MPa)	S_o/S
–	0	1300	16.2	35.0	10	19	25.0	88	43.0	3.50
1	4	1490	16.1	32.5	8.5	20	25.9	76	35.0	2.95
	15	1700	15.8	25.8	4.5	25	22.5	57	30.7	2.53
	20	2000	16.0	25.0	2.8	20	21.0	43	23.7	2.05
	28	2350	16.0	22.9	2.2	16	19.7		19.6	1.70
	36	2520	16.1	19.4	1.3	1.6	17.0		16.7	–
2.5	4	1470	15.8	32.1	8.3	21	27.0	83	36.0	3.0
	15	1700	15.9	25.3	7.3	33	21.2	63	29.8	3.03
	20	2020	16.3	22.3	4.9	23	21.0	41	24.4	1.93
	28	2210	16.2	20.2	3.1	20	19.6		19.8	1.63
	36	2260	15.6	16.6	1.2	1.6	14.8		15.0	1.34
8	4	1400	16.0	32.0	8.3	22	25.3	75	32.5	2.95
	15	1760	16.0	25.5	5.8	27	23.7	58	25.2	2.45
	20	2000	16.1	24.0	5.6	40	22.6	41	23.8	1.80
	28	2130	15.1	18.0	4.8	22	17.6		17.6	1.57
	36	2230	14.1	15.5	4.2	20	15.5		15.5	1.05
	47	2160	13.8	12.0	1.4	18	11.5		11.4	1.03
25	4	1430	14.9	31.0	6.7	21	25.8	69	29.1	2.68
	15	1670	11.6	25.0	6.6	37	22.6	43	23.2	1.91
	20	1800	9.1	22.4	7.0	42	22.2	33	22.8	1.48
	28	2040	8.2	17.2	6.8	–	17.2		17.7	1.30
	36	2170	7.6	15.4	6.8	–	15.4		16.2	1.03
	47	1670	6.6	11.0	7.0		11.0		11.8	1.02

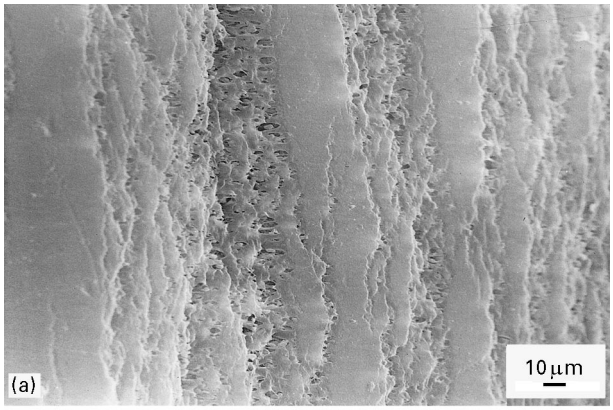

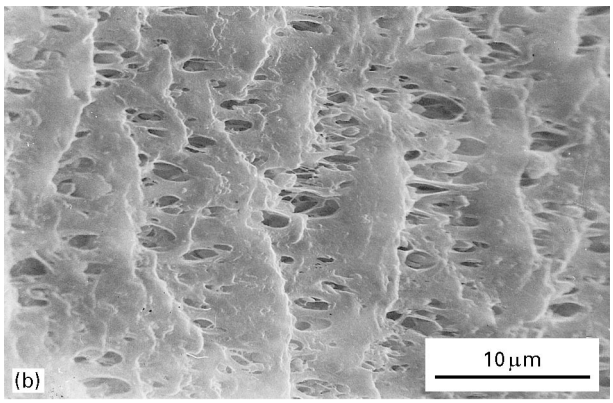

Figure 4 SEM micrographs of the surfaces of the deformed compositions, containing 28 vol % of a filler with $\bar{d} = 1$ μm. (a) magnification: ×280, (b) ×2100.

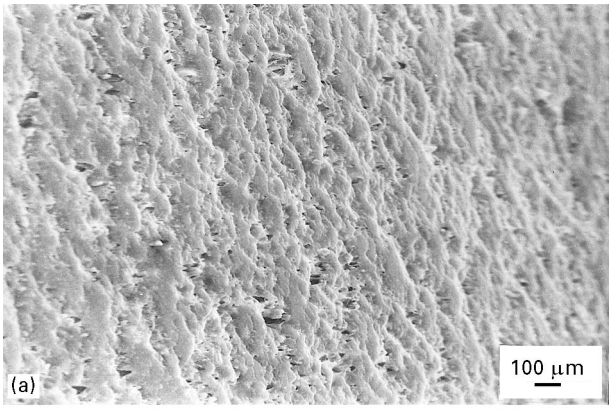

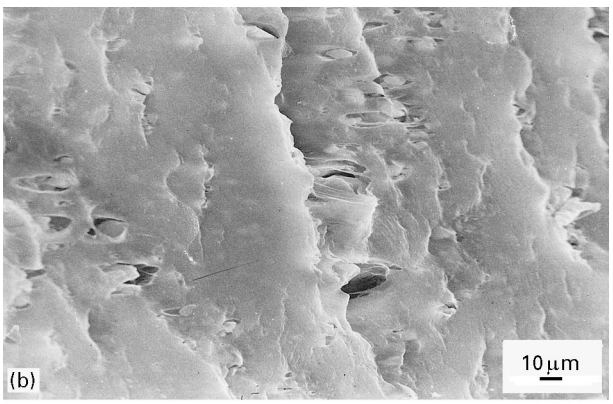

Figure 6 SEM micrographs of the surfaces of the deformed compositions, containing 28 vol % of a filler with $\bar{d} = 25$ μm. (a) Magnification: ×42, (b) ×280.

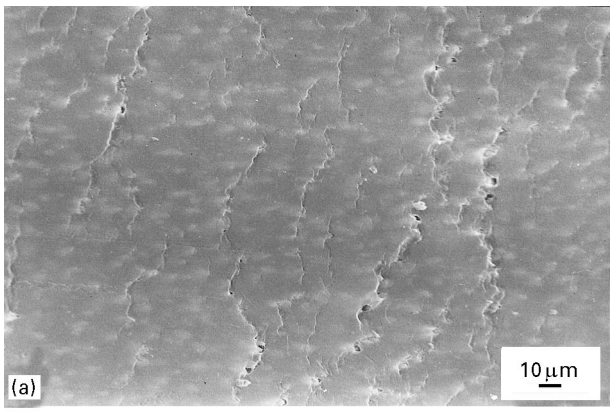

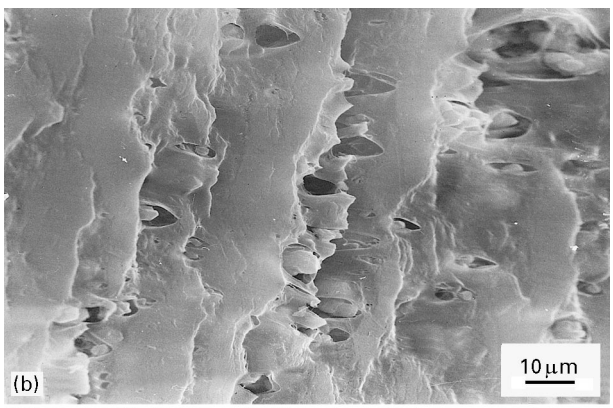

Figure 5 SEM micrographs of the surfaces of the deformed compositions, containing 28 vol % of a filler with $\bar{d} = 8$ μm. (a) magnification: ×280, (b) ×700.

(Figs. 4b, 5b and 6b) indicate that the narrow plastic zones have a craze-like structure with micro pores, nucleated by debonded particles. Any opening of the pores and corresponding local strains are noticeably smaller than the ones contained in the neck in the samples with low filler contents (Figs 3b).

Sharp localization in a short neck of a whitened region is typical in the case of small particles (Figs 2c and 4a). The amount of these zones outside this region is very low. In the case of large particles ($\bar{d} = 8$ and 25 μm) sharp macroscopic localization of plastic flow does not occur. Simultaneous nucleation of numerous narrow craze-like zones and an extended region of whitening is visually observed for the samples containing 28 vol % of rigid inclusions. Uniform whitening and macro homogeneous deformation are distinctive features for the specimens with $\phi = 36$ vol % (Fig. 2b). The microstructure of the samples is characterized by a high concentration of micro porous zones and their uniform disposition all over the volume (Figs. 5a and 6a).

To conclude this section we would like to highlight that changes in the composites yielding behaviour with an increase in the filler fraction are caused by a transition from a micro homogeneous to a craze-like mechanism.

The following questions need to be addressed:

(i) What are the reasons for the observed transition and which parameters are responsible for the critical value ϕ_{cr}?

(ii) Why is different ultimate elongation behaviour observed in regions 1 and 2 and how is this related to the size of the inclusions?

The explanations that will be proposed in the following sections are based on an understanding of the influence of the debonding micro processes on the composite materials mechanical behaviour.

3.3. The effect of dispersed phase content on the deformation mechanism of the composites with nonideal adhesive bond: the reason for the transition from a micro homogeneous to a craze-like mechanism

The systems under investigation are characterized by a rather weak adhesive interaction. Thus, the nucleation of micro pores, caused by debonding, occurs at the initial stages of the loading. An increase of the inclusion content results in the inclusions coming closer together and the exfoliation along the surface of one of them significantly affects the change of the stress–strain state (SSS) in its neighbourhood. The dependence of the relative distance (l/r) between inclusion surfaces (r being an inclusion radius) on ϕ is listed in Table II. This data was calculated using a geometrical model based on identical balls located in the sites of a cubic lattice. The maximum relative normal stresses ($k = \sigma/\sigma_0$ – stress intensity) as a function of the distance from the spherical pore are listed in Table II (σ_0 being the axial stress at infinity). It can be observed, that k significantly increases with a decrease of the relative distance above l/r values of 0.8, which corresponds to $\phi \simeq 20$ vol %. For $\phi < 20$ vol % the extra stress does not exceed 10%, i.e., in region 1 the particles are sufficiently remote from each other that no noticeable correlation between deformation processes in their vicinities occurs and formation of specific deformation clusters does not occur.

At $\phi > 20$ vol % (region 2) debonding of one of the inclusions essentially changes the SSS of its neighbours. Maximum stresses are realized in the planes of the pore equators, transverse to the direction of the loading. Thus exfoliation along the surfaces of particles causes nucleation and growth of micro porous craze-like zones perpendicular to the drawing axis. The formation of such structures during the initial stage of deformation was experimentally revealed in the SEM studies (Fig. 7(a and b)). The effects of this mechanism become more strongly pronounced with a decrease in the distances between inclusions, i.e., with a further increase in the filler content.

Thus, the transition from a micro homogeneous to a craze-like mechanism corresponds to a transition from independent to correlated micromechanical processes. This occurs in the vicinity of different inclusions due to an increase of the stress intensity factor which results from a diminution of the distance between inclusions.

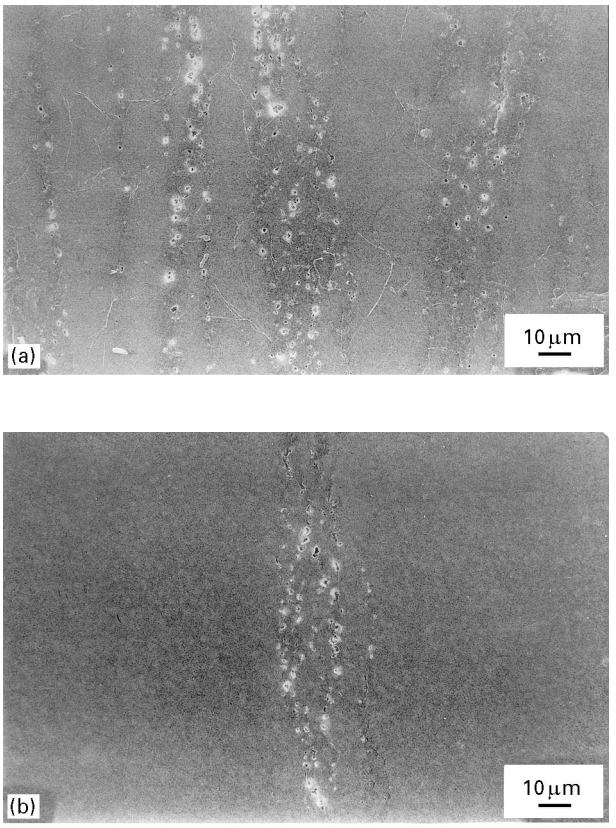

Figure 7 SEM micrographs of the craze-like clusters in a composite sample surface at the initial stage (before plastic flow) of deformation for (a) $\phi = 28$ and (b) 36 vol %, $\bar{d} = 2.5$ μm.

3.4. The relationship between filler content and size and plastic deformation and fracture behaviour in the regions where (1) micro homogeneous and (2) craze-like mechanisms apply

3.4.1. The analysis of the initial portion of the stretching diagrams as a method for the identification of debonding processes

A study of adhesive failure at low filler content ($\phi = 0.5$ vol %, $\bar{d} = 8$–150 μm) has been reported on model systems [9, 10]. In these cases the debonding precedes plastic flow of the polymer and an increase in the particle size results in a drop in the debonding stresses.

The relationships between the debonding micro processes during the initial stages of the loading and

TABLE II Stress intensity k in the elastic matrix, caused by a spherical pore of radius r, at a distance l from its surface

ϕ (%)	2	4	10	15	20	25	30	35	40	45
l/r	3.94	2.71	1.47	1.03	0.76	0.56	0.41	0.29	0.19	0.10
k	1.00	1.01	1.02	1.05	1.09	1.15	1.23	1.34	1.48	1.67

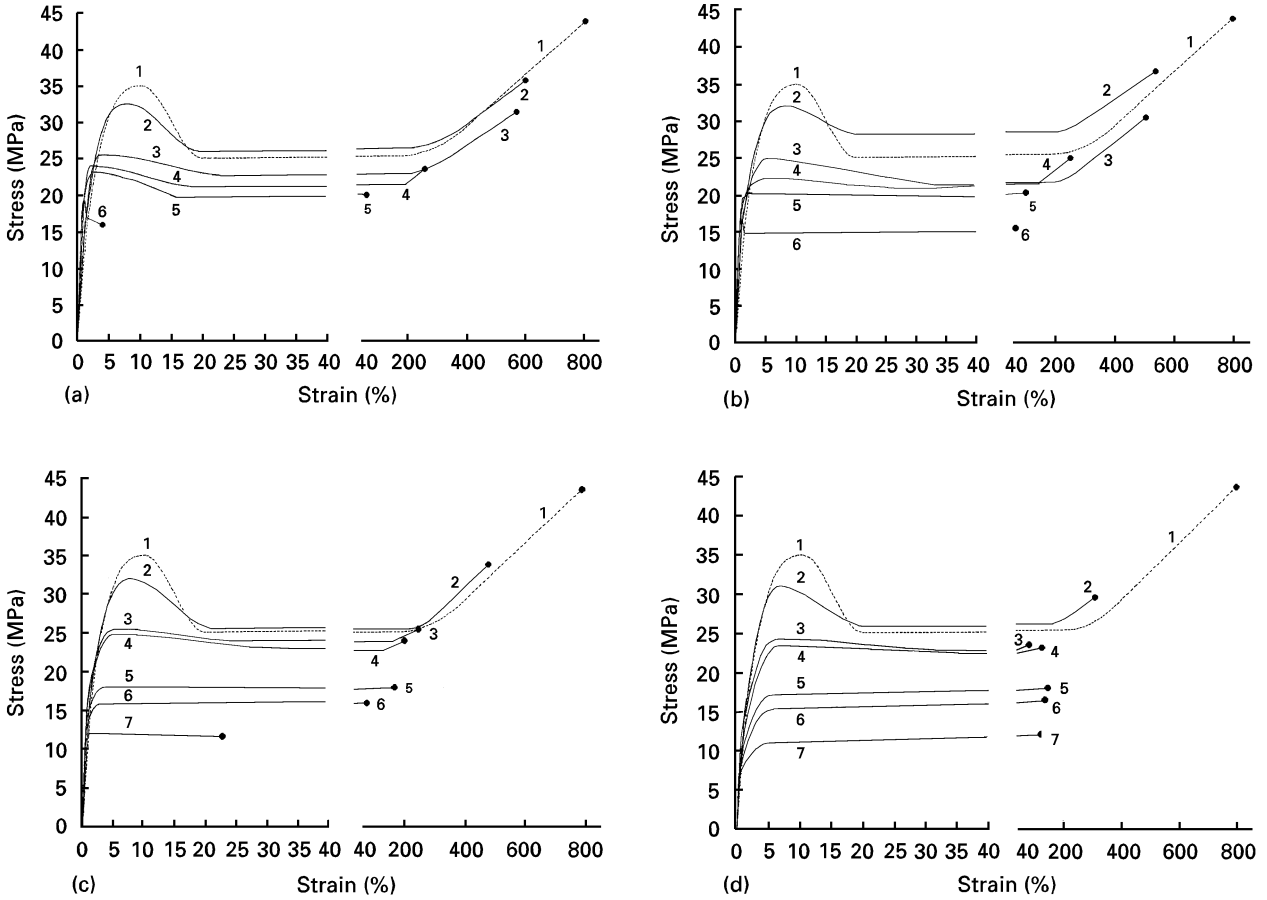

Figure 8 Stretching diagrams of PP–$Al(OH)_3$ composites. (a) $\bar{d} = 1$, (b) 2.5, (c) 8 and (d) 25 μm, $\phi = 0$ (curve 1), 4 (curve 2), 15 (curve 3), 20 (curve 4), 28 (curve 5), 36 (curve 6) and 47 (curve 7) vol %.

mechanical behaviour of the composites at large deformations were not investigated in the studies of references [9, 10], but they are the subject of the present paper. The optical method used in reference [10] is not applicable to real composites with small particles and high filler content. That is why the conclusions of this paper, concerning particle content and size effects on the nucleation and growth of micro pores in the PP–$Al(OH)_3$ system, are based on the analysis of changes in the initial sections of stretching diagrams and also SEM observations of the microstructure of the deformed sample.

The stretching diagrams for the composite are shown in Fig. 8(a–d). The elastic moduli (E) (initial slopes), elastic limits (σ_e, linear ranges), yield stresses (σ_y) and strains (ε_y), the stresses (σ_{pl}) and strains (ε_{pl}) of the exit on the plateau were determined from Fig. 8. The data obtained are summarized in Table I. The cross-sectional area ratios (S_o/S), true stresses in the necks (σ_n^{tr}) and ultimate stresses (σ_b) are also reported in Table I.

It can be seen that the inclusions size does not noticeably affect the composites elastic behaviour. A certain tendency for a decrease in the modulus at a high (about 50 vol %) content of large ($\bar{d} = 25$ μm) particles is the only exception. This is probably caused by the presence of initial defects in the structure.

The data of Table I show that the values σ_e for the composites do not differ from the matrix one in the case of small particles ($\bar{d} = 1$ and 2.5 μm). A diminution in σ_e as compared with a matrix value is observed at $\phi > 20$ vol % for inclusions of size $\bar{d} = 8$ μm and at an arbitrary ϕ for $\bar{d} = 25$ μm. The existence of an initial common behaviour on the diagrams for different $\bar{d}$ at fixed ϕ is clearly seen from Fig. 9(a and b). It is natural to assign the deflection of the diagrams from the linear behaviour to the beginning of the debonding events. The drop in the corresponding stress values with the increase in the particle diameters coincides with the results presented in references [9, 10].

Fig. 8(a–d) also demonstrates a decrease in the composite yield stress (σ_y^c) with filling. In accordance with the model of Nilsen [1] for the effective cross-sectional area, the drop in σ_y^c with an increase in ϕ may be described by the equation:

$$\sigma_y^c = \sigma_y^m(1 - \alpha\phi^{2/3}) \quad (1)$$

assuming that a weak adhesive interaction is in operation. σ_y^m is a matrix yield point and the parameter α accounts for partial transmission of the load to the particles.

The data for σ_y^c are listed in Table I. In region 1 ($\phi < 20$ vol %) they are consistent with Equation 1 for every $\bar{d}$ that has the same value of α, corresponding to complete debonding. This means that at low filler contents, debonding occurs for the majority of particles before the matrix yield point is reached, independent of their size. If ϕ exceeds 20 vol % (region 2), the influence of the filler size on the composites yield point

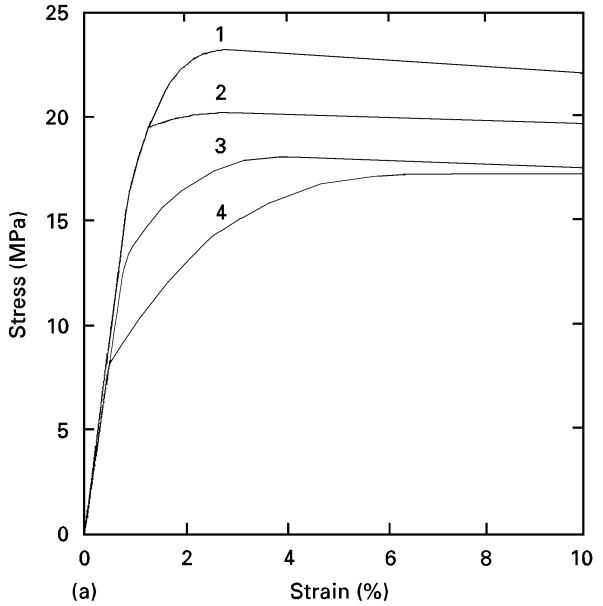

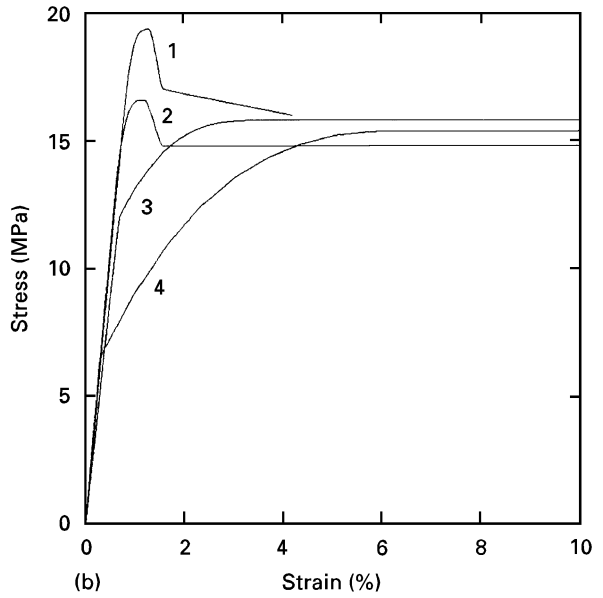

Figure 9 Initial portions of PP–$Al(OH)_3$ composites stretching diagrams. (a) $\phi = 28$ and (b) $\phi = 36$ vol %, $\bar{d} = 1$ (curve 1), 2.5 (curve 2), 8 (curve 3) and 25 (curve 4) μm.

becomes more noticeable. The behaviour of σ_y^c may also be described by Equation 1, but α drops with a decrease in $\bar{d}$. This is probably caused by a decrease in the concentration of debonded particles.

3.4.2. Characteristic features of the stretching diagrams in the region of plastic flow and fracture

Before the analysis of the features of the tension diagrams above the yield point and, in particular, of the ultimate properties, it is sensible to discuss the general nature (macro homogeneous or localized) of material plastic deformation. Let us consider two hypothetical types of engineering diagrams (a stretching force, divided by an initial cross-section versus relative elongation) under the condition of homogeneous stretching (the scheme of Fig. 10). If it continuously increases (curve 1), i.e., a unique value for the strain is produced

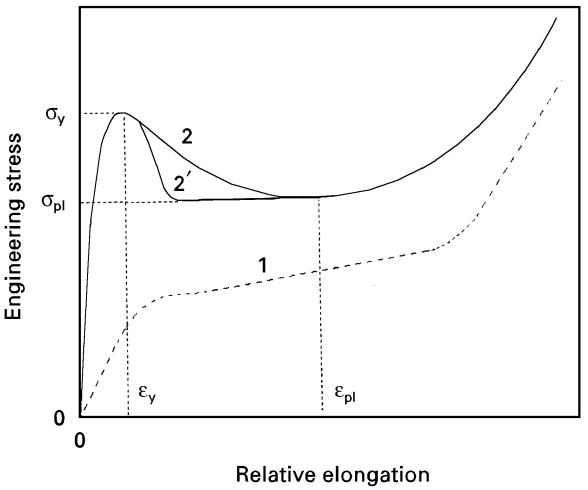

Figure 10 Schematic representation of (1) monotonous and (2, 2′) extreme type stretching diagrams. 2 – unstable homogeneous deformation, 2′ – deformation with necking.

by an applied force, then localization of the deformation cannot take place. In the case of extreme behaviour typified by curve 2, homogeneous flow becomes unstable for stretching above the maximum and formation of a macro inhomogeneity (a neck) becomes energetically advantageous (curve 2′). Local elongations at the neck are determined by the position of the minimum on curve 2. The second stage of the sample deformation is the propagation of the neck by the drawing into it of new portions of weakly deformed regions. The corresponding part of the curve is parallel to the elongation axis. This process will be terminated by the breakage of the sample in the case of no or only insignificant strain hardening (zero or only a low difference between the stresses σ_b and σ_{pl}). On the other hand, the neck will continue to be developed if the value $\sigma_b - \sigma_{pl}$ is significant and then the third stage – homogeneous strain hardening – will occur. The values and the positions of the maxima and minima should be almost the same for curves 2 and 2′. Thus, experimentally found stresses and strains of yielding and necking may be regarded as the maximum and minimum points on the hypothetical homogeneous diagrams which can be realized only under special conditions due to their instability.

If the true stresses increase with drawing (such a situation holds for the currently studied materials), an absence or presence of maxima on the engineering diagrams should be determined by the intensity of cross-sectional area during the drawing process. The less the growth of the sample volume, the more significant is a change in cross-sectional area.

Let us analyse the PP and PFP plastic flow behaviour from this point of view. The deformation of unfilled PP occurs in an heterogeneous manner, the neck is characterized by a decrease in size in the transverse direction ($S/S_0 = 3.5$) and the stretching diagram is of an extreme type (Fig. 8, curve 1). This means that no noticeable change in the sample volume occurred during the deformation. Adhesive failure in the particulate filled composites leads to the formation of pores. The higher the pore concentration, the more intense is

the growth of the sample volume in the drawing process.

In region 1 of the microhomogeneous mechanism the tension diagrams are of the extreme type. This means that at $\phi < 20$ vol % the pore concentration is insufficient to change the nature of the diagrams and the composites continue to deform by necking (Fig. 8, curves 1–3). However, an increase in the filler fraction leads to a decrease in the ratio σ_y/σ_{pl} (Table I) and thus to a tendency of homogeneous flow.

In this region all the volume of the composite specimen is drawn into the neck with subsequent strain hardening (the composite containing 15 vol % of particles of size $\bar{d} = 25$ μm, is the only exception to this behaviour) (Fig. 8). The ultimate strain and stress diminish with both an increase in ϕ and $\bar{d}$ (Fig. 1). The pore fraction in the sample at the yielding stage grows with ϕ because of the complete debonding. The presence of the pores causes heterogeneous SSS. The stress-strain distribution and the values of ultimate strain for PFP were calculated by Gorbunova *et al.* [2] on the basis of small elastoplastic deformations in a periodic structure, which implies a micro homogeneous mechanism. The model predicts a rise in the stress concentration in the material with an increase in ϕ and a corresponding diminution of ε_b. The drop in the value of the ultimate strain in the present case of large deformations is probably caused by the same effect.

The observed decrease in ε_b with an increase in $\bar{d}$ in region 1 is consistent with a general law of a drop in the strength properties with a growth in the size of a defect. A corresponding quantitative model for PFP brittle fracture was proposed by Oshmian [11]. The proposed explanation of the drop in strength is based on the increase in size of dangerous concentration zones with an increase in particle diameter. The decrease in ε_b with the filler size in the case of composites based on superplastic matrixes is probably governed by an analogous mechanism. An additional influence of the filler size on the PFP ultimate strain may be caused by the polymer nature of matrix. The smaller the size of the particles, the greater the specific free surface of the micro pores. An intuitive assumption concerning the rise of mobility for a macromolecule close to the free surface is an argument for the observed increase of ε_b with the diminution of $\bar{d}$.

In region 2, which is controlled by a craze-like mechanism of yielding ($\phi > 20$ vol %) an essential difference between the materials with small and large inclusions is observed in the character of the diagrams. The cases of localized flow ($\bar{d} = 1$ and 2.5 μm) are characterized by the conservation of the yielding peak and its narrowing with an increase of ϕ (ε_{pl} goes to the left: Table I, Figs 8(a and b) curves 5, 6). Quasi-brittle fracture at $\phi = 36$ vol % occurs with the formation of a very short neck and the diagrams that correspond to this behaviour are characterized by an extremely narrow peak (Fig. 9b). However in the cases of homogeneously deformed composites ($\bar{d} = 8$ and 25 μm) an increase in the filler fraction results in the diminution of $\sigma_y - \sigma_{pl}$, in the widening of the peak (ε_{pl} goes to the right: Table I) and in its eventual disappearance (Figs. 8(c and d) curves 5–7; Fig. 9).

SEM observations of the specimen surfaces just before the start of macroscopic flow was performed. In the case of small particles ($\bar{d} = 1$, 2.5 μm) a sharp drop in the density of craze-like zones inside the plastic flow region with an increase in filler fraction was established (Fig. 7). On the other hand, an increase in the concentration of the craze-like zones was observed in the case of large particles ($\bar{d} = 8$, 25 μm).

The represented data support the following conclusions. The yield peak width coincides with concentration of microporous bands forming at the start of macroscopic flow. The concentration of craze-like zones is small in the case of localized macroscopic flow and rather large in the case of macro homogeneous deformation. The increase in the concentration of microporous zones causes a smaller drop in the cross-sectional area in the drawing process. As was discussed previously, this factor promotes the narrowing of the difference between the maximum and minimum in the engineering diagrams, which is the reason for the tendency for macro homogeneous flow. As long as the craze-like zones carry the larger part of the deformation the increase of their density should produce an increase in the ultimate strain due to at least two reasons: (i) the increase of the concentration of intensively deformed regions and (ii) the decrease of strain rates inside them.

The manner of the transition from localized to macro homogeneous flow in highly filled PP and the rise of ε_b, alternative to the increase of the inclusion size, was discussed by Dubnikova *et al.* [12]. In this work a modification of the interface by silicone liquid, which lowers adhesive interactions was investigated. The dependence of the ultimate strain on filler size is shown in Fig. 11(a and b) for both the cases of non-modified (curve 1) and modified (curve 2) particle surfaces for $\phi = 28$ vol % (Fig. 11a) and 36 vol % (Fig. 11b). It is seen that the encouragement of debonding changes the character of the flow (from localized to macro homogeneous) and essentially increases the ultimate elongation for the compositions, filled by small particles. In the case of large inclusions ($\bar{d} = 8$ μm and 25 μm), when macro homogeneous flow occurs without the modification, the treatment of the surface has only a minor effect on ε_b.

Thus in a craze-like mechanism the influence of the filler size on the composite flow and fracture behaviour is mainly determined by a change of adhesive failure conditions.

3.4.3. The influence of debonding stress values on the concentration of craze-like zones

Zhuk *et al.*, [10] have shown that there exists a range of debonding strengths $\sigma_{dmin} < \bar{\sigma}_d < \sigma_{dmax}$ for every given particle diameter. The first debonding events begin after the achievement of σ_{dmin}. A single debonding causes the exfoliation of its neighbours and the formation of craze-like zones. The pore concentration inside the craze should be close to ϕ, and therefore specific cross-sectional area of the matrix polymer layers (bulkheads) may be estimated by the

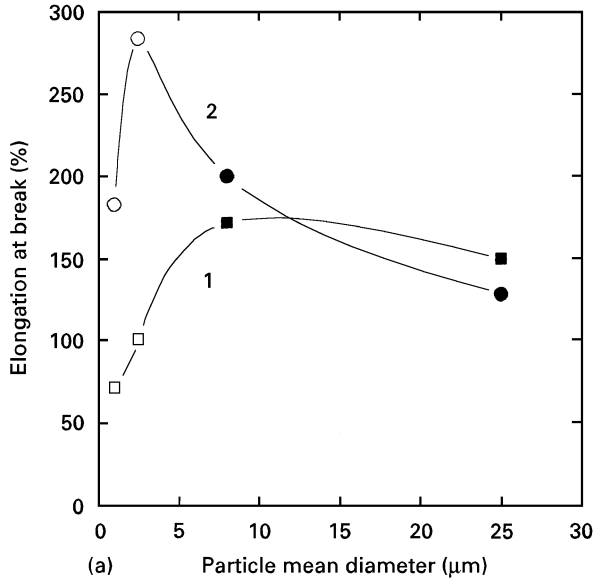

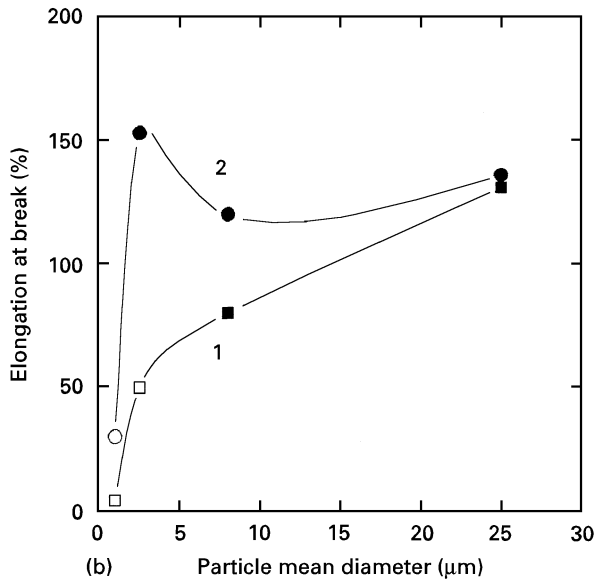

Figure 11 ε_b dependence on particle size for highly filled (1) unmodified and (2) modified PP–$Al(OH)_3$ composites at (a) $\phi = 28$ and (b) $\phi = 36$ vol %. Macromechanism of deformation: localized (hollow) and homogeneous (filled) flow.

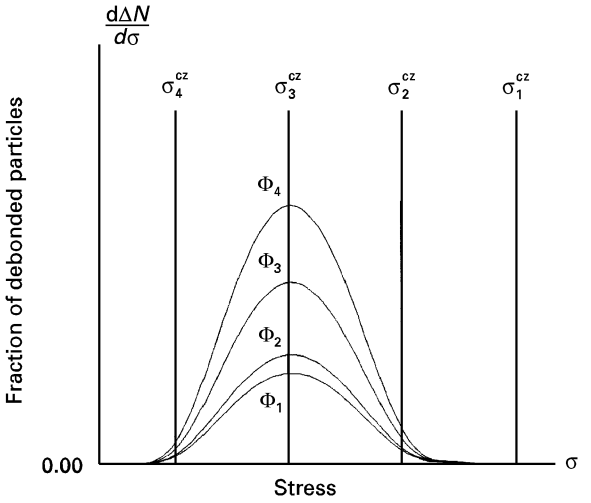

Figure 12 Schematic representation of debonding stress distribution for fixed $\bar{d}$ at different ϕ, $\phi_1 < \phi_2 < \phi_3 < \phi_4$.

value $1 - \alpha\phi^{2/3}$. Let us denote the stress in the bulkheads by σ^{bh}. Then the walls of the craze are tightened by the stress σ^{cz}

$$\sigma^{cz} = \sigma^{bh}(1 - a\phi^{2/3}) \quad (2)$$

Further exfoliation in the vicinities of the walls occurs only if σ^{cz} exceeds σ_d and the concentration of debonded particles (ΔN_d) and thereby the craze-like zones are determined by the relationship between σ^{cz} and σ_d. The amount of debonding occurring in the stress interval between σ and $\sigma + d\sigma$ is equal to $(d\Delta N_d/d\sigma)\, d\sigma$ and the resulting value of ΔN_d is determined by the integral:

$$\Delta N_d = \int_{\sigma_{dmin}}^{\sigma^{cz}} \frac{d\Delta N_d}{d\sigma}\, d\sigma \quad (3)$$

The character (homogeneous or localized) of the composite macrodeformation is determined by the density of microporous zones at the stage of yielding. Let us first examine the value of ΔN_d at the condition $\sigma^{bh} = \sigma_y^m$ as a function of ϕ at a fixed σ_d. We will use the debonding stress distribution schematically shown in Fig. 12 and relabel the variable σ^{cz} as σ_y^{cz}, which is solely a function of ϕ. The areas of the peaks are proportional to ϕ, and their positions do not noticeably change and σ_y^{cz} (vertical lines on Fig. 12) decreases with ϕ in accordance with Equation 2. Three characteristic regions should be discussed.

1. $\sigma_y^{cz} > \sigma_{dmax}$. In this region of ϕ, the upper limit in the integral in Equation 3 may be replaced by σ_{dmax}, therefore all particles are debonded and ΔN_d rises proportionally with the filler fraction, which creates the macro homogeneous character of the flow.

2. $\sigma_y^{cz} \simeq \sigma_{dmin}$. This condition creates a small number of craze-like zones which produce a sharp localization of macroscopic yielding and quasi-brittle fracture.

3. $\sigma_{dmin} < \sigma_y^{cz} < \sigma_{dmax}$. In this region the area of the peaks (Fig. 12) remain proportional to ϕ, however the relative fraction of debonding particles drops. Competition between these two factors should cause an extreme ΔN_d–ϕ dependence. The decrease in the concentration of craze-like zones leads to a tendency for localized flow, which occurs at a certain value ϕ_{loc}. It is natural to consider ϕ_{loc} to be a transitional point from plastic to quasi-brittle fracture ($\phi_{br} = \phi_{loc}$), because it corresponds to the sharp drop in ultimate elongation (Fig. 1).

Let us analyse the particle size effect (which is the factor that determines $\bar{\sigma}_d$) on the character of the ΔN_d–ϕ dependence. As previously mentioned, σ_y^{cz} is independent of $\bar{d}$, however debonding stresses fall with an increase in particle diameter. This should result in an increase in the macro homogeneous flow region and an increase in ϕ_{br}. Experimental data confirm these predictions: ϕ_{br} is slightly above ϕ_{cr} for $\bar{d} = 1, 2.5$ μm, $\phi_{br} \simeq 36$ vol % for $\bar{d} = 8$ μm and $\phi_{br} > 47$ vol % for $\bar{d} = 25$ μm.

Thus, the low debonding stress values are associated with macro homogeneous flow at high ϕ (region 2) in the case of large particles. The increase of ultimate strain for $\bar{d} = 25$ μm at 15 vol % < ϕ <

35 vol % (Fig. 1, curve 4) is probably caused by an increase in the concentration of craze-like zones in this region of ϕ.

The high debonding stress values cause the localization of macroscopic yielding in the composites with small particles at ϕ_{br} values slightly above ϕ_{cr}. As the deformation process proceeds, the conditions for new zone formation will be reached after the achievement of a strain hardening state for the bulkheads inside the neck. An essential difference between the micro porous zone concentration inside and outside the neck is confirmed by the SEM data (Fig. 4a). The decrease of the craze strength (the value derived in Equation 2 with σ_b for the bulkheads) with ϕ results in the decrease in the amount of newly formed zones and a decrease in ε_b.

The craze screening effect causes incomplete debonding not only at the yielding stage, but also just ahead of the breaking of the bulkheads. The ultimate strain may be roughly estimated as the value proportional to the craze concentration in all of the sample length. This may be expressed as the product $c^{cz}L$, where c^{cz} is the craze concentration and L is the sample length in the case of macro homogeneous deformation or the length of the neck in the case of localized flow. The encouragement of adhesive failure (by the use of a particle diameter increase, for instance) simultaneously leads to the growth of both c^{cz} and L due to the transition from localized to homogeneous yielding. This is the reason for an increase of ε_b with an increase in $\bar{d}$ at $\phi \geqslant 28$ vol % (Fig. 1) in contrast to region 1 that has a microhomogeneous mechanism. The deviation from this behaviour in the vicinity of the left boundary of region 2 (compare curves 3 and 4 of Fig. 1) may be explained by a competition between a craze-like mechanism at ϕ close to 20 vol % and a decrease in ultimate properties with an increase in pore size, which is suitable for region 1 as was previously discussed.

4. Conclusions

The conclusions are as follows:

(1) An experimental study of the plastic deformation mechanisms for particulate filled polymers has been performed on PP–$Al(OH)_3$ containing a filler with sizes ($d = 1$, 2.5, 8 and 25 μm) and in concentrations up to 47 vol%.

(2) A critical filler content, $\phi_{cr} \simeq 20$ vol %, for the transition between two micromechanisms and a change in the macroscopic laws for plastic flow in composite was discovered. The transition from independent at $\phi < \phi_{cr}$ to correlated at $\phi > \phi_{cr}$ micro debonding events is the main reason for a change in mechanism.

(3) Below ϕ_{cr} the composite yielding behaviour occurs in a micro homogeneous way on the scale of the inclusion size or distance. Engineering stretching diagrams are of the extreme type and sample drawing occurs macro heterogeneously with the formation and propagation of a neck. The ultimate elongation decreases with an increase in filler size.

(4) Above ϕ_{cr} plastic deformation occurs micro heterogeneously: the main part of the total deformation is concentrated inside the narrow craze-like zones with polymer layers between debonded particles acting as bulkheads. These zones are transverse to the drawing direction. In the case of small particles their density is very low which results in the localization (necking) of macro deformation and quasi-brittle fracture. In the case of large filler size craze-like zones density is high, stretching diagrams are monotonous and the character of deformation tends to the macro homogeneous one. Ultimate strains increase with filler size in the range considered. The values of ε_b mostly drop with ϕ, however for $d = 25$ μm there exists a region of growth (15–35 vol %). The change of adhesive failure conditions with filler size, mainly a decrease in debonding stress is seen as the main reason for the PFP plastic flow behaviour described in this work.

Acknowledgements

We acknowledge the financial support provided by the Russian Foundation of Fundamental Research, Project No. 93-03-18609 and also by the award of a grant from the William and Mary Greve Foundation.

References

1. L. E. NIELSEN, "Mechanical Properties of Polymers and Composites". (Marcel Dekker, New York, 1974).
2. N. V. GORBUNOVA, N. N. KNUNYANTZ, V. A. TOPOLKARAEV, L. I. MANEVICH and V. G. OSHMIAN, *Mekhanika Kompoz. Mater.* (1990) 336.
3. V. A. TOCHIN, E. N. CSCHUPAK, V. V. TUMANOV, O. V. KULACHINCKAYA and M. I. GAY, *ibid.* (1984) 635.
4. I. L. DUBNIKOVA, A. I. PETROSYAN, V. A. TOPOLKARAEV, YU. M. TOVMASYAN, I. N. MESCHKOVA and F. S. D'YACHKOVSKII, *Vysokomol. Soyed.* **A30** (1988) 2345.
5. V. A. TOPOLKARAEV, N. V. GORBUNOVA, I. L. DUBNIKOVA, T. V. PARAMZINA and F. S. D'YACHKOVSKII, *ibid.* **A32** (1990) 2210.
6. I. L. DUBNIKOVA, V. A. TOPOLKARAEV, T. V. PARAMZINA, E. V. GOROKHOVA and F. S. D'YACHKOVSKII, *ibid.* **A32** (1990) 841.
7. M.PEGORARO, A. PENATY, E. CAMMARATA and M. ALIVERTI, in "Polymer blends: Process, Morphology and Properties" (Plenum, New York 1984) Vol. 2, p. 205.
8. V. A. TOPOLKARAEV, YU. M. TOVMASYAN, I. L. DUBNIKOVA, A. I. PETROSYAN, I. N. MESCHKOVA, A. A. BERLIN, YU. P. GOMZA and V. V. SCHILOV, *Mekhanika Kompoz. Mater.* (1987) 616.
9. N. N. KNUNYANTZ, A. V. ZHUK, V. G. OSHMIAN, V. A. TOPOLKARAEV and A. A. BERLIN, *Mackromol. Chem., Macromol. Symp.* **44** (1991) 295.
10. A. V. ZHUK, N. N. KNUNYATZ, V. A. TOPOLKARAEV, V. G. OSHMIAN and A. A. BERLIN, *J. Mater. Sci.* **28** (1993) 4595.
11. V. G. OSHMIAN, *Mekhanika Kompoz. Mater.* (1992) 34.
12. I. L. DUBNIKOVA, E. V. GOROKHOVA, A. YA. GORENBERG, V. A. TOPOLKARAEV, *Vysokomol. Soyed.* **A37** (995) p. 1535.

Received 8 August 1995
and accepted 21 May 1996